Synthesis and characterization of carboxylic-and amine-grafted FAU zeolites as inorganic fillers to design biocompatible composites

Thomas Menard, Baylar Zarbaliyev, Aline Echalard, Erika Bullier-Marchandin, Fanny Gens, Guy Ladam, Benoît Louis, Gaëtan Lutzweiler

Synthesis and characterization of carboxylic- and amine-grafted FAU zeolites as inorganic fillers to design biocompatible composites

Thomas Menard, Baylar Zarbaliyev, Aline Echalard, Erika Bullier-Marchandin, Fanny Gens, Guy Ladam, Narmina Guliyeva, Benoît Louis, Gaëtan Lutzweiler**

1- Univ Rouen Normandie, INSA Rouen Normandie, CNRS, PBS UMR 6270, F-76000 Rouen, *France*
2- ICPEES-UMR 7515, Université de Strasbourg, CNRS, 25 rue Becquerel, F-67087 Strasbourg, France
3- Azerbaijan State Oil and Industry University, ASOIU, 16/21 Azadliq Ave, Baku, Azerbaijan

Keywords: Faujasite; composites; Gelatin Hydrogel; Surface Functionalization; macrophages

Highlights:

- Surface functionalization of FAU via APTES or TESPA allowed to graft either amine or carboxylate groups, to mediate their covalent incorporation into a gelatin hydrogel.
- Thermal properties of the resulting composites were substantially improved compared with non-crosslinked conditions.
- The FAU/gelatin composites were found biocompatible with respect to macrophage-derived THP-1 cells.

Abstract

Zeolites have been used for decades in industry owing their large surface area, high stability and well-defined crystalline structure. Therefore, numerous synthesis routes have been developed to tune the morphology and the physical chemical properties of the final zeolite. In particular in the biomedical field, zeolites were used as drug carriers, and even as transporters to penetrate directly into the cells. The aim of this study was to develop zeolite-based composites which involved a gelatin matrix covalently bonded to zeolites. Nanosized faujasites (FAU) were synthesized leading to a colloidal suspension prior to mixing with gelatin solutions at different FAU-to-gelatin weight percentages. FAU morphologies and size distribution were investigated by SEM and DLS focusing on the aggregation propensity in response to different pH and ionic strength. Zeolite surfaces were then functionalized to graft either amine, or carboxylic groups, using the well-known 3-(aminopropyl)triethoxysilane (APTES) for amine, and 5-(triethoxysilyl)pentanoic acid (TESPA) for carboxylic groups for the first time. According to these strategies, zeolites were covalently linked to gelatin chains via EDC/NHS coupling widely used in biology. The successful surface functionalization was assessed by ATR-FTIR, XPS, and zeta potential measurements. The resulting composites were found stable under physiological temperature compared to gelatin alone, as confirmed by DSC analysis. Lastly, in order to get a first glimpse of the potential use of these composites in biology, gels were incubated in culture media prior to be poured onto macrophage-derived THP-1 cells, showing good viability. FAU zeolite crystals could therefore be used as fillers to improve thermal properties of gelatin hydrogels, using a novel surface functionalization strategy, being thus promising candidates as scaffolds for tissue engineering, or even wound dressing.

1. Introduction

The development of composite materials has attracted much attention in the last decades, which results from the combination of two components, typically a polymer, with nano/micro particles, in order to leverage their properties synergistically. For instance, advanced thermoplastic composites based on polyamides have been used for aerospace applications for more than 50 years[1]. Several aspects of the resulting composites can be controlled which encompasses mechanical, thermal, optical, or electrical properties. More recently, carbon nanonotubes have attracted much attention when combined with polymers, yielding to light and cheap materials with enhanced electrical conductivity[2]. In biology, most composites are implemented as scaffold for tissue engineering applications. Usually the particles are intended to improve the mechanical properties of the polymer matrixes which are poorly stable under shearing, or load bearing conditions[3], or as drug delivery systems. Composites are widespread in nature and in living organisms gathering seashells or bones, which are composed of inorganic crystals surrounded by a collagenous matrix. Such anisotropic systems are highly complex exhibiting structural features at various length scales, and artificial reproduction of such systems remains largely iterative rather than rationalized[4]. Nevertheless, several efforts have been made in that purpose, seeking for an efficient selection of the polymer matrix, along with the dispersed particles with satisfying complementarity.

A promising candidate for biological applications is gelatin which derives from either alkaline, of acid hydrolysis of collagen, being itself, a component of several tissues including cartilage or skin. Gelatin is cell adherent, no cytotoxic, and biodegradable owing to its specific amino acid sequences. Moreover, gelatin can spontaneously form a gel, due to a coil-to-helix transition, at temperatures near 30 °C, which is however limiting for *in vivo* applications. Besides, the mechanical properties of such hydrogels are also quite poor, due to the high hydration degree, and the weak bonds stabilizing the triple helix assembly. Chemical crosslinking can in part circumvent these issues using glutaraldehyde, transglutaminase, or genipin among others[5]. Clays have been widely used as fillers in composites due to their high aspect ratio, which can serve as crosslink points for hydrogels[6,7], thus reinforcing the mechanical properties of the materials. Another example is iron oxide nanoparticles, allowing to design drug delivery systems controlled by an external magnetic field[8]. Zeolites are crystalline aluminosilicates gathering more than 250 identified structures, with five of them being key players in the industry gathering sorption, laundry, catalysis, up to the lenses of the Range Rover robot[9] on March. Zeolites are obtained from the self-assembly of aluminate and silicate precursors around a structure directing agent (SDA) driving the formation of cavities, channels and cages with regular dimensions. The rationalization of their synthesis allows to precisely control their pore dimension from micropores (< 2 nm) to mesopores (2 – 50 nm) which was performed by introducing for instance hard templates during the synthesis[10].

The size of the crystals can be tuned by proper selection of the synthesis route, whereby the balance between crystal nucleation and growth rate can be modulated by temperature or alkalinity[11]. Moreover, Awala *et al*.[12] successfully produced nanosized zeolites with sodium ion acting as SDA, which is of prime interest for biological applications, since sodium ions are abundant and non-toxic unlike quaternary ammonium usually used as SDA. The high porosity and related surface area of zeolites can be leveraged to load ions or molecules targeting specific biological applications. Likewise, sustained drug delivery was achieved for cancer treatment and imaging[13], modulation of pre-osteoblastic cells fate[14], or to introduce antimicrobial features[15]. Moreover, nanosized zeolites are subject to endocytosis, for instance to deliver 5-fluorouracil into breast cancer cells[16], and nitric oxide inhibitor into THP-1 cells[17].

Considering the significant payload that can be introduced into zeolites, along with their apparent biocompatibility, their introduction in composite systems could reinforce the gel strength and thermal stability depending on the zeolite / polymer matrix interactions, thus playing the role of inorganic filler, and as a drug delivery system simultaneously.
To date, only few studies combined zeolites with polymer matrixes, and zeolites were dispersed into a crosslinked polymer without directly interacting with the polymer chains. For instance, Mittal *et al.*[18] developed a hydrogel made from karaya gum crosslinked via adding *N*-isopropylacrylamide (NIPAM) to react with acrily acid, into which FAU crystals were dispersed throughout, and other systems including polysaccharides or proteins were designed following the same approach[19].
Herein, FAU crystals will be synthesized to be dispersed into a gelatin matrix, to produce biocompatible composites. The main goal will be to incorporate covalently FAU into a biocompatible hydrogel, in order to improve the thermal properties of gelatin. FAU exhibits a low silicon-to-aluminum ratio (SAR) and adapted channel and super cage sizes (1.3 nm), allowing for the storage of active compounds, it is biocompatible, and colloidal suspensions can be obtained according to the synthesis route, using non-toxic sodium ion as SDA[13]. Direct covalent bridging between gelatin and FAU zeolite will be achieved after surface modification of zeolites for the first time, and thoroughly characterized. Two surface groups will be grafted namely amines, and carboxylates to investigate a larger panel of choices to produce the composites. On one hand, amine groups will be grafted onto the external surface of FAU (NH_2-FAU) by reacting silanol groups with common (3-aminopropyl)triethoxysilane (APTES). On the other hand, carboxylate groups will be incorporated via functionalization with 5-(triethoxysilyl)pentanoic acid (TESPA), leading to COOH-FAU, which to the best of our knowledge, was not reported yet. The covalent linkages with gelatin will eventually be achieved via the classical *N*-(3-Dimethylaminopropyl)-*N*'-ethylcarbodiimide (EDC) / *N*-hydroxysulfosuccinimide sodium (NHS) coupling, widely used in biology. EDC/NHS treatment promotes the reaction between carboxylic acids and amines, since both groups are found in gelatin, one can expect that the FAU-gelatin linkages will be built at different location of the protein depending whether COOH-FAU, or NH_2-FAU will be used. Finally, cytotoxicity assays will be performed to probe their influence on the viability of macrophage-derived THP-1 cells.

2. Experimental

2.1. Materials

2.1.1. Nanosized zeolite synthesis and functionalization

Faujasite type zeolites were synthesized using the method already described by Awala *et al.*[12] Briefly, polypropylene (PP) bottles were washed with ultrapure water. The final solution was prepared at molar ratio of 9 Na_2O : 0.7 Al_2O_3 : 10 SiO_2 : 160 H_2O. A first solution (1) was prepared by incorporating 0.649 g of sodium aluminate (Sigma, CAS: 11138-49-1) into 4 mL of ultrapure water, followed by 0.5 g of NaOH. Solution (2) was also prepared in PP bottles, adding 11.32 g sodium silicate (Sigma, CAS: 6834-92-0) in 3.4 mL of ultrapure water with 1.25 g NaOH. Solutions were stirred with a magnet bar until transparent solution was obtained. Solution (2) was placed in an ice bath and stirred vigorously until the solution became viscous, then solution (1) was poured dropwise into (2. The subsequent aging phase was conducted at 25°C for 24 h, under stirring at 350 rpm. Finally, the hydrothermal crystallization phase was carried out at 50°C for 45 h in an oven.

At the end of the reaction, the solutions containing the zeolites produced were analyzed by dynamic light scattering (DLS), before washing in order to diminish both pH and ionic strength. Washing steps consisted in centrifugation of zeolite containing solution at 10 000 rpm for 5 min, the supernatant was then removed and replaced with fresh phosphate buffer saline (PBS). Up to 10 washing steps were performed. Finally, zeolites were recovered and left to dry at room temperature.

Surface functionalization of zeolites was carried out using two functionalizing agents: (3-aminopropyl)triethoxysilane (APTES, Merck, CAS: 919-30-2) to yield amine-grafted faujasites (FAU-NH_2) and 5-(triethoxysilyl)pentanoic acid (TESPA, Merck, CAS: 1137665-94-1), to graft carboxylic groups onto the zeolite surface (FAU-COOH). FAU-NH_2 were prepared by adding 2.5 g of neat zeolites (FAU) suspended in 50 mL ethanol, then, 5 mL or 10 mL APTES was added yielding to a 10 % or 20 % APTES solution. The mixture was heated for 24 h at 80°C under stirring at 300 rpm in a flask under reflux.
For the synthesis FAU-COOH, the same set-up was used: 2 g of FAU were dispersed in a solution containing 9 mL of pure ethanol was mixed with 1 mL TESPA which was dissolved beforehand, in order to work under anhydrous conditions. The solution was heated up at 80°C for 24 h. The zeolites were collected by centrifugation and washed with ultrapure water 3 times, then neutralized by further washing cycles with PBS 10x (Dulbecco's Phosphate Buffer Saline, Corning) until reaching a pH 7. Zeolites were then dried at room temperature.

2.1.2. Composite preparation

Composites were prepared in solutions containing 15 wt.% type A gelatin from porcine skin (Sigma, gel strength 300, CAS: 9000-70-8), and 15 wt.% of either FAU, FAU-NH_2, FAU-COOH in ultrapure water. Gelatin solutions were prepared at 28 wt.% in PBS at 60°C. In 2 mL Eppendorfs, 0.2 g of zeolites were deposited, before adding either 0.23 mL of 2-(N-morpholino)ethanosulfonic acid buffer (MES), or MES buffer with *N*-(3-Dimethylaminopropyl)-*N*'-ethylcarbodiimide (EDC) (Merck, CAS: 1892-57-5)/ *N*-hydroxysulfosuccinimide sodium (NHS) (Merck, CAS: 106627-54-7). The resulting mixture was homogenized for 30 min in an ultrasonic bath, then heated at 60°C before mixing with supercooled gelatin at 4 °C. For a 1.33 g hydrogel, the composition consists in 0.2 g gelatin, 0.7 g PBS, 0.2 g zeolites, and 0.23 g buffer with the corresponding crosslinking. The mixtures are left for aging at 60°C for 4h for amidation reaction to take place, before being left at room temperature for gelation.
The crosslinking solutions based on the EDC/NHS combination were prepared in 10 mL of MES buffer, by adding 1 mL (EDC), and 0.434 g NHS, under gentle stirring for 15 min, then poured in contact with FAU-COOH or FAU-NH_2, for 30 min under gentle stirring in a 1:1 ratio.

2.2. Instrumental measurements

2.2.1. The X-ray photoelectron spectroscopy (XPS)

X-ray photoelectron spectroscopy measurements were performed in an ultrahigh vacuum (UHV) spectrometer equipped with a VSW SCIENTIFIC hemispherical electron analyser. The Al Kα hν=1486.6 eV dual anode X-ray source was used as incident radiation. The constant pass energy mode was used to record both survey and high-resolution spectra, with pass energies 90 and 22 eV respectively.

2.2.3. Dynamic Light Scattering (DLS)

Zeolite particle size was determined using a Malvern Zetasizer Nano DLS instrument. This analysis was carried out using zeolite suspension in ultrapure water, then in water with PBS 10x at variable concentration to pH 7. The incident beam wavelength is 633 nm.

2.2.4. X-ray powder diffraction (XRD) analysis

X-ray diffraction patterns were recorded on a Bruker D8 Advance diffractometer equipped with a Ni detector side filtered Cu Kα radiation (1.5406 Å) over a 2θ range of 5-55 degrees. The analysis of crystal structure has been conducted by choosing a step of 0.02° and an acquisition time of 0.5 s to get the detailed peak analysis of powder zeolite samples.

2.2.5. N_2 sorption analysis (BET)

The textural properties involving the BET surface area (S_{BET}) were evaluated from classical nitrogen physical adsorption–desorption isotherms measured at 77 K by means of ASAP2020M equipment (Micromeritics). Prior to analysis, the zeolite samples (100 mg) were outgassed at 150°C for 7 h to remove water molecules or impurities present in the pores.

2.2.6. Scanning electron microscopy (SEM)

SEM images were obtained with a Zeiss GeminiSEM 500 microscope with a FEG Schottky source and an Everhart–Thornley detector. The microscope has been operated at different electron high tension (EHT) voltages ranging from 2 to 6 kV. Prior to observation, the zeolite surface has been coated with gold for 120 s at 20 mA by using a Quarum QT1307—039 instrument.

2.2.7. Zeta potential analysis

The zeta potential was obtained by measuring electrophoretic mobility, then using the Smoluchowski equation.

2.2.8. ATR-FTIR spectroscopy

Spectra were obtained using a Thermo Scientific Nicolet iN10 MX instrument, the blank was atmospherically corrected, and a check was made with non-functionalized zeolites to identify peaks resulting from surface functionalization steps. The resolution chosen for spectra acquisition was 2 cm^{-1}. Zeolite samples were desiccated prior to FTIR.

2.2.9. Thermal stability test

Gels were poured at over 60°C into 24-well plate wells to obtain a flat surface, then left to gel overnight at room temperature. The gels obtained are placed in an oven at 37°C, and turned upside down at different times. If the gels did not flow under gravity, they were considered stable, and subsequently incubated in culture medium (RPMI, ATCC) also at 37°C, to determine their stability using the same methodology.

2.2.10. Differential scanning calorimetry

DSC thermograms were acquired with a DSC 92 instrument (SETARAM) apparatus. Composites were weighted before each analysis, and placed into a closed 120 μL aluminum crucible. Each scan was conducted from 25 to 45 °C in order to visualize the effect of each treatment on the gel-sol transition of gelatin. Heating rate was fixed at 2 °C.min^{-1}.

2.3. Investigation of biological properties of composites

Cell culture and viability assessment

THP-1 human monocytic cells (TIB-202, ATCC) were grown in 75 T-flasks containing RPMI-1640 (ATCC) media supplemented with 10% v/v fetal bovine serum (ATCC) and 1% v/v penicillin/streptomycin, placed in an incubator (37 °C, 5 %, CO_2). Before seeding, culture media were changed every 3-4 days. At passage number 15, cells were seeded at a density of 500 000 cells per mL at the bottom of 48 well plates with 500 µL of the fresh medium with Phorbol 12-myristate 13-acetate (PMA) at 50 μM (Sigma, CAS: 16561-29-8) to differentiate THP-1 into macrophages for 7 days. In triplicate, 150 mg of EDC/NHS-cross-linked hydrogel of gelatin (FAU), gelatin with FAU-NH2, and gelatin with FAU-COOH were immersed in 500 µL of fresh medium for a few seconds on day 1, then 24 h on day 2, and so on until day 6 to evaluate the influence of by-products released from the composites, after functionalization and crosslinking steps. The collected medium (500 µL / well) and fresh medium solely for the control conditions (500 µL / well) were poured on the macrophages for 24 h before performing an Alamar blue® (BUF012B, Bio-rad) test. The viability of the cells following the instructions was provided by the manufacturer. Briefly, culture media were removed and replaced with a mixture of fresh culture media supplemented with the 10% v/v Alamar blue® reagent, and incubated for 3 hours in the dark. Afterwards, 100 µL were pipetted in each well and transferred into a 96 well-plate prior to measurements at 570 and 600 nm using a microplate reader (Synergy 2, Biotek Instruments, Inc.). The reduction percentage of Alamar blue® was calculated from the absorbance values at 570 and 600 nm using the following equation:

$$\text{Percentage reduction of Alamar blue: } = ((O2 \cdot A1) - (O1 \cdot A2))/((R1 \cdot N2) - (R2 \cdot N1)) \quad (1)$$

where O1 = 80 586 and O2 = 117 216 are the molar extinction coefficients of oxidized Alamar blue at 570 and 600 nm, respectively (values provided by the manufacturer); R1 = 155 617 and R2 = 14 652 are the molar extinction coefficients of reduced Alamar blue also at 570 and 600 nm. A1 and A2 are the absorbance values of the samples at 570 and 600 nm, while N1 and N2 are the absorbance values of negative controls (i.e. media with Alamar blue without cells). The test was carried out from day 1 to day 6.

3. Results and discussion

3.1. Synthesis and characterization of composites

FAU zeolites have been synthesized using sodium ion as a template following the methodology described by Awala *et al.*[12] The main advantage of this route being the absence of potentially harmful organic structure directing agent (SDA), but also the nanosize of the resulting crystals. The sole presence of the FAU structure could be confirmed from the XRD pattern (**Figure 1a**) as attested by the position of the Bragg's peaks[20], along with some amorphous materials detected by the hump in the baseline[21]. This uncomplete crystallization can be explained by the short hydrothermal treatment (45 h), but neither phase impurity (such as LTA or EMT), nor mixture of phases could be evidenced[22]. The resulting crystals exhibited the classical octahedral morphology of FAU (**Figure 1b and Figure S4**) with typical size in the range of roughly 90-100 nm. Despite the nanosized dimension of individual crystals, aggregation occurred rapidly after synthesis. DLS measurements were performed in order to determine the diameter of FAU aggregates (**Figure 1c**), leading to particle of 5-10 μm in diameter directly after synthesis. Such phenomena can arise from the high concentration of alkaline metal ions used during synthesis. As described in classical colloid theory, their stability is tightly related to the ionic strength, whereby repulsive effects due to electrostatic forces and osmotic pressure are favored under low salt concentration[23]. Moreover, the initial formation and dispersion of zeolite precursors is important, as it controls their crystallization kinetics ultimately leading to

larger crystals. Although related to ion mobility, the molar conductivity can reflect the ionic strength of a given solution[24]. Likewise, in this study, sodium and hydroxide ions are the most abundant as attested by the pH ~ 13 (**Figure S1**). Hence, in order to get closer from the physiological conditions, several rinsing steps in phosphate buffer saline (PBS) were performed to decrease the pH value, and the ionic strength simultaneously. It can be observed in **Figure 1c** that the first rinsing step affected only slightly the size distribution, despite appearance of particles of 270 nm. The ionic conductivity was almost divided by two after the first rinsing step (from 34 000 to 18662 μs) (**Figure 1d**). Measuring the ionic conductivity can be relevant to assess colloidal stability of nanosized zeolites or their potential dissolution as highlighted by Gözcü *et al.*[25] After the fifth rinsing, the size of aggregates was smaller but quite broad lying in the range of ~ 200 nm to 1.5 μm. Furthermore, the evolution of ionic conductivity was also much less pronounced (from 180 to 107 μS), suggesting that the medium was mainly composed of PBS. This indicates that several washing steps were suitable to obtain smaller aggregates.

The synthesis of isolated crystals is challenging, for instance, most of zeolite synthesis are performed by using an organic structure directing agent (SDA) such as tetrapropylammonium (TPA), driving the self-assembly of zeolite precursors. However, TPA usually leads to the formation of larger aggregates as discussed by Kirschhock *et al.*[26] Also, high alkalinity favors the formation a large number of nuclei giving particles of smaller size, as shown for nanosized silicalite-1[27], and FAU. After 5 washing steps, the size of aggregates hereof was in the order of hundreds of nanometers, which was considered as satisfactory for the purpose of this study. Noteworthy, crystals can be sorted via centrifugation to get particles in the range of 15 – 90 nm (**Figure S2**), but the number of zeolites harvested is quite limited, and it is also more difficult to control the weight percentage of zeolite relative to gelatin by this mean.

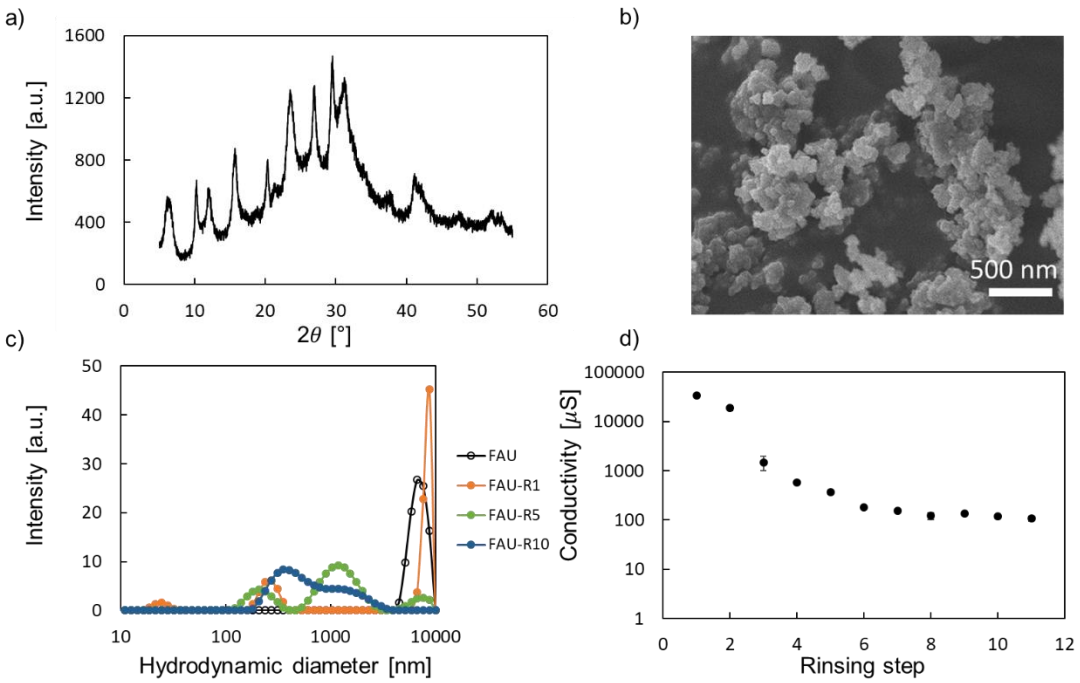

Figure 1. a) XRD pattern of as-obtained pristine FAU crystals. b) SEM image showing FAU aggregates following synthesis. c) Determination of the hydrodynamic diameter of FAU crystals without rinsing (FAU), one rinsing step (FAU-R1), five (FAU-R5), and 10 rinsing steps (FAU-R10). d) Evolution of the conductivity as a function of the number of rinsing steps in PBS buffer.

As a first attempt to produce gelatin/zeolite composites, a combinatorial screening of various gelatin (5, 10, 15 %) and zeolites (0, 0.1, 0.5, and 1 %) concentrations was performed (**Figure 2**) in order to determine whether a given formulation would be stable at 37 °C. The relative amount of zeolite to polymer is an important parameter to control Young's modulus or swelling properties. For example, Zhang *et al.*[28] found that 10 % loading of FAU into hydrogel contributes to increase the shear modulus by 100 %, but weakens at larger concentrations. Moreover, the hydrophilic nature of zeolites increases the swelling ratio of alginate up to a certain alginate-to-zeolite ratio[29]. Regarding gelatin-zeolite composites, early work of Ninan and co-workers[30] revealed that 0.5 % FAU allowed for a larger increase in Young's Modulus, as well as an improved resistance against degradation into aqueous media. The authors related such effect to the electrostatic interactions between zeolites and gelatin. Herein, preliminary thermal stability tests displayed in **Figure 2** indicate that none of the tested conditions were enough to stabilize the composites, suggesting minor interactions between zeolites and gelatin. This could be explained by the fact that gelatin, despite bearing some charges, is highly hydrated as well as zeolites, whose surface harbors silanol groups at neutral pH. Accordingly, highly solvated particles may not interact each other, which require another strategy to promote gelatin-zeolites interactions.

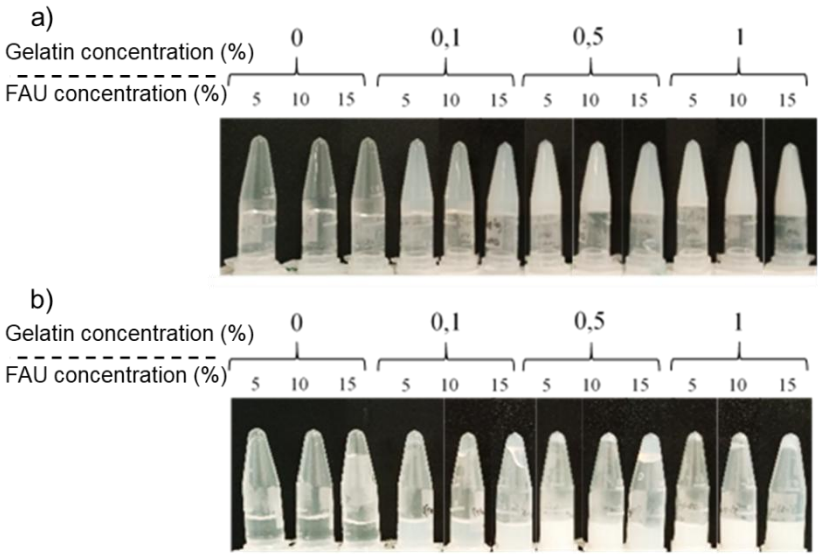

Figure 2. Thermal stability tests of gelatin/FAU composites at 37 °C. Tubes were turned upside down, and conditions where gels hold at the top were considered stable. Images were taken at t= 0h (a), and t = 24 h (b).

Two different strategies were undertaken to graft either amine or carboxylic groups on the external surface of FAU crystals. The zeolite surface was modified using organoalkoxysilanes to insure a covalent bonding. For this work, APTES ((3-aminopropyl)triethoxysilane) was selected at first. Thanks to its free amine group[31], it has been widely employed for the functionalization of mesoporous silica, but also recently to functionalize nanozeolites, to further catalyze the formation of pyrrol derivatives[32]. Furthermore, the cell-recognized RGD sequence could be grafted onto zeolite LTL crystals, after amination by APTES[33]. On the other hand, carboxy-modified FAU was obtained by reaction of surface silanol 5-(triethoxysilyl)pentanoic acid (TESPA), inspired by the work of Feinle *et al.*[34] on silica particles. Other alternatives were employed to graft carboxylic groups for instance using di-carboxylic acids (oxalic, or succinic

acid)[35].
The grafting mechanism is based on the hydrolysis of the alkoxy groups (-Si-(O-Et)$_3$) of silanes to produce hydrogen bond accepting sites which further enable adsorption, to be stabilized on the zeolite surface, due to the silanol groups predominantly present. Finally, condensation between hydroxylated silanes and zeolite silanols is possible, enabling organosilanes to be covalently grafted to zeolites[36,37] (**Figure 3)**.

The uniformity of the grafting of trialkoxysilane depends on the proximity of the silanol groups. If they are close enough, a maximum of two alkoxy functions may react on the surface[38]. However, direct condensation between the alkoxysilanes rather than with the surface silanols is also likely. Of note, the hydrolysis step is carried out mainly at the zeolite surface, since the reaction was carried out in absolute ethanol, only the presence of adsorbed water molecules at the zeolite surface could hydrolyze alkoxysilanes[39,40].
Unlike mesoporous silica, the presence of Al in the zeolite framework may act as a spacer between silanol groups reducing condensation between neighboring alkoxysilanes[41].

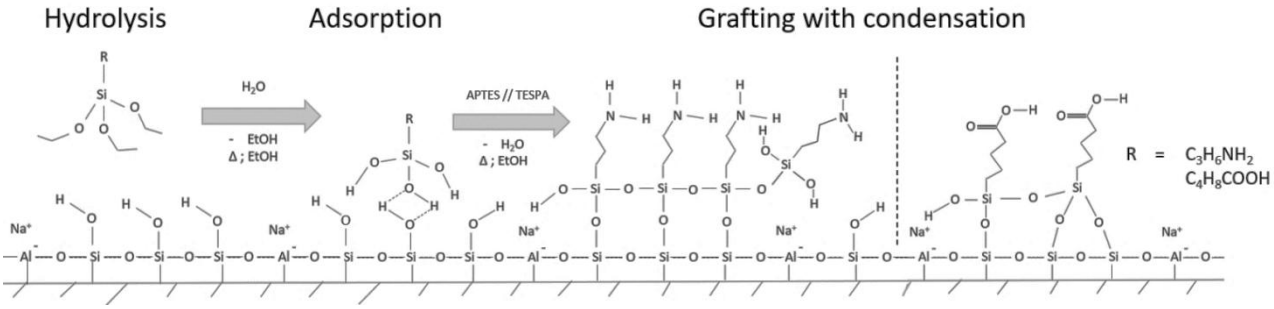

Figure 3. Three-step reaction scheme for grafting APTES (left hand side with respect to the dashed line) and TESPA (right hand side with respect to the dashed line) onto zeolite surfaces.

ATR spectra of neat zeolites (FAU) and aminated FAU (FAU-NH_2) are shown in **Figure 4a**. FAU treated with APTES (i.e. FAU-NH_2) exhibited distinct bands at 3720 cm^{-1}, and 1530 cm^{-1} respectively assigned to amide II and N-H bonds of primary amine[42], which are absent in pristine FAU. Moreover, two other small bands at 2900, and 2980 cm^{-1} appeared which can be ascribed to $CH_2CH_2CH_2$–NH_2 groups[43]. This confirmed that amine groups could be grafted onto zeolites surfaces. Furthermore, specific surface area was calculated from N_2 adsorption isotherms (**Figure S3**), displaying a marked reduction (from 679 $m^2.g^{-1}$ to 200 $m^2.g^{-1}$), implying that some pore entrance were blocked by the external surface modification. Considering the small pore dimensions of FAU (0.74 nm[43]), it is unlikely that APTES (molecule length of 0.5- 1 nm[44]) could diffuse into the FAU framework, but instead, steric hindrance of organosilanes may repel N_2 gas molecules from the inner part of zeolites.
Since primary amines are positively charged under neutral pH, the zeta potential of FAU-NH_2 may shift from negative values owing to the presence of silanol groups (isoelectrical point $\sim$2[45]) to more positive ones. Unmodified FAU exhibited a zeta potential in the range of $\sim$ -30 mV (**Figure 4b**), which is in the limit of the generally admitted threshold value of $\pm$ 30 mV required to stabilized colloidal suspensions[46]. The solutions were stable for weeks with only minor sedimentation. A strong shift could be observed for FAU-NH_2 which harbored a zeta potential of 22.13 mV. This value is in the same order than was has been found by Vilaça et al.[16] for lysine-coated LTL zeolites (+ 32 mV), and Mahmoodi and co-workers[47] (+ 17.9 mV) for APTES treated SOD zeolite. Higher concentrations of APTES did not yield to higher surface charges (data not shown).

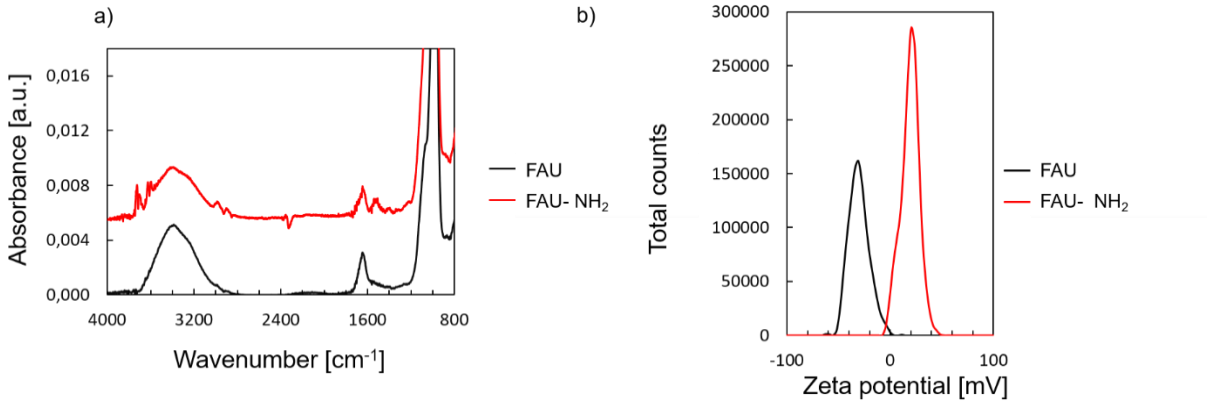

Figure 4. a) FTIR-ATR spectra of FAU and amine-grafted FAU (FAU-NH_2), and b), measurement of zeta potential of FAU and FAU-NH_2 dispersed in PBS buffer.

Regarding carboxylated FAU (FAU-COOH), ATR spectra between FAU, and FAU-COOH were nearly identical (**Figure 5a**) excepted the appearance of a slight peak at 1563 cm^{-1}, which can be attributed to the stretching of carboxylate group[48]. Interestingly, specific surface area was only slightly reduced (i.e. 648 $m^2.g^{-1}$) (**Figure S3**) compared to FAU, which could indicate that the grafting density is less than for FAU-NH_2, although being confirmed too. Zeta potential shifted toward more negative values (from – 30 mV to -45 mV) (**Figure 5b**), which indicates at least a modification in surface charges. Lu *et al.*[49] recorded a zeta potential of -25 mV following carboxylation, but zeolites were loaded with Tris(bipyridine)ruthenium(II), ($Ru(bpy)_3^{2+}$), providing additional positive charges, and thus, increasing the zeta potential. In another study, carboxylation of LTL zeolites led to a surface potential of – 50 Mv[50] instead of – 39 mV for neat zeolites. Overall, zeta potential provides a quantitative mean to confirm surface modifications of colloidal zeolites, but the absolute value is related to the number of external silanol groups, and the nature of functionalizing molecules, which can explain the observed differences with the literature.

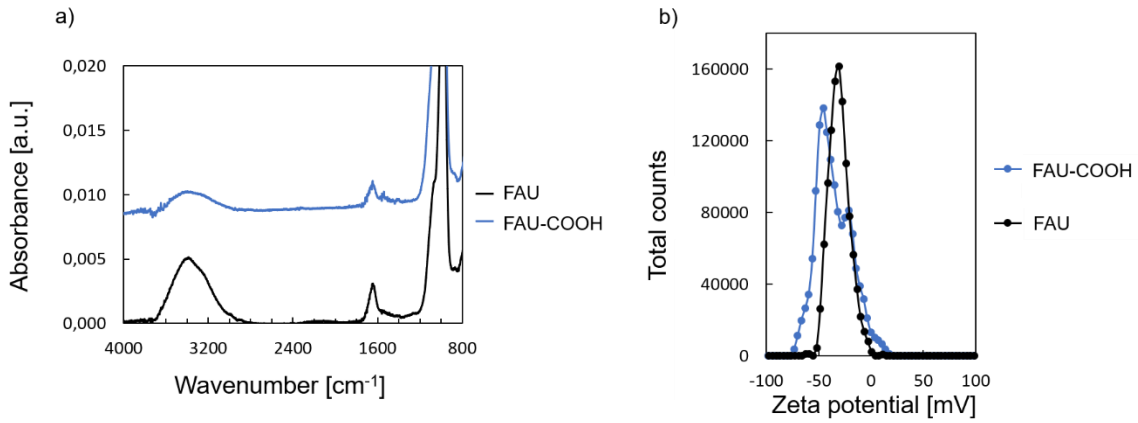

Figure 5. a) FTIR-ATR spectra of FAU and carboxylated FAU (FAU-COOH), and b), measurement of zeta potential of FAU and FAU-COOH dispersed in PBS buffer.

Consequently, a quantitative probing of surface elements was performed through XPS analysis, for both C1s, O1s, and N1s (Figure 6). APTES treatment resulted in a marked increase of the peak intensity at 286 eV assigned to carbon atom (Figure 6a), for FAU-NH_2 in comparison with pristine FAU. Moreover, nitrogen (401 eV) could only be detected in FAU-NH_2 sample; neither for FAU, nor FAU-COOH (**Figure 6b**) which further confirmed the grafting of the amine. This trend is in good agreement with other studies with APTES-modified zeolites[51], and with APTES-modified SiO_2 whose surface is enriched in silanol as for zeolites[52]. Grafting of carboxyl groups is also evidenced from **Figure 6a** and c, whereby the carbon signal is the strongest for FAU-COOH which can be related to the number of carbon atoms of the aliphatic chain of TESPA (4) while 3 C are present on APTES (FAU-NH_2). Assuming that both alkoxy groups of both APTES and TESPA have reacted at the same extent, the amount of carbon differs only from the aliphatic chain bearing the amine/carboxylic group. From Figure 6c, the peak at 530 eV results from an overlap from three contributions, namely, the O-T oxygen from the zeolite framework where T denoted either Si or Al, the C=O, and C-O[53]. Peaks of surface-modified zeolites are shifted toward smaller binding energy, the most pronounced being for FAU-COOH, which is attributed to an increase contribution of C=O bonds from carboxylic groups. The small shift visible for FAU-NH_2 can be related to C-O bond, which indicates that all the three alkoxy groups of APTES did not bind to zeolite but only partially, leaving some free alkoxy groups. Of note, surface functionalization had no effect on the XRD pattern (**Figure S5**).
With all these data in hand, we have tempted to estimate the grafting density or, more likely, the degree of external surface modification. According to literature, a density of approximately 2 O-H / nm^2 could be assessed for Y zeolite by Kawai *et al.*[54] whereas slightly less than 1 O-H / nm^2 could be estimated for bare silica[55] herein, the external surface area determined by BET analysis for pristine FAU, was 232 m^2 / g. As 0.2 g of zeolite was typically used to produce a composite, a surface of $4.6.10^{19}$ nm^2 is available, thus leading to $1.1.10^{20}$ surface silanol groups (0.17 mmol). If we assume a complete grafting of either APTES or TESPA, as both may react with 3 ethoxy groups (Figure 3), a coverage of 59 μmol of APTES/TESPA for 0.2 g of zeolite could be expected (in an ideal case).

After integration of the curves corresponding to the C_{1s} signal in **Figure 6**, a ratio between $C1s_{NH2\text{-}FAU}$ and $C1s_{COOH\text{-}FAU}$ of about 0.6 is obtained. According to their chemical structure, TESPA has 4 carbon atoms whilst only 3 are present in APTES, thus, at equivalent grafting density, one would expect a ratio of 0.75. Regarding the textural properties, the dramatic loss in the specific surface area in NH_2-FAU sample compared with COOH-FAU (**Figure S3**), one can reasonably

suggest a more efficient grafting density for COOH-FAU sample. In addition, its textural properties remained the same after the external surface functionalization step, with the same micropore volume and specific areas values than pristine FAU zeolite, thus being encouraging for further biological applications. In stark contrast, the micropore volume almost completely vanished for NH_2-FAU, indicating pore blocking, probably due to a non-homogeneous grafting process of APTES. Furthermore, these large differences in textural properties can result from a different grafting mechanism.

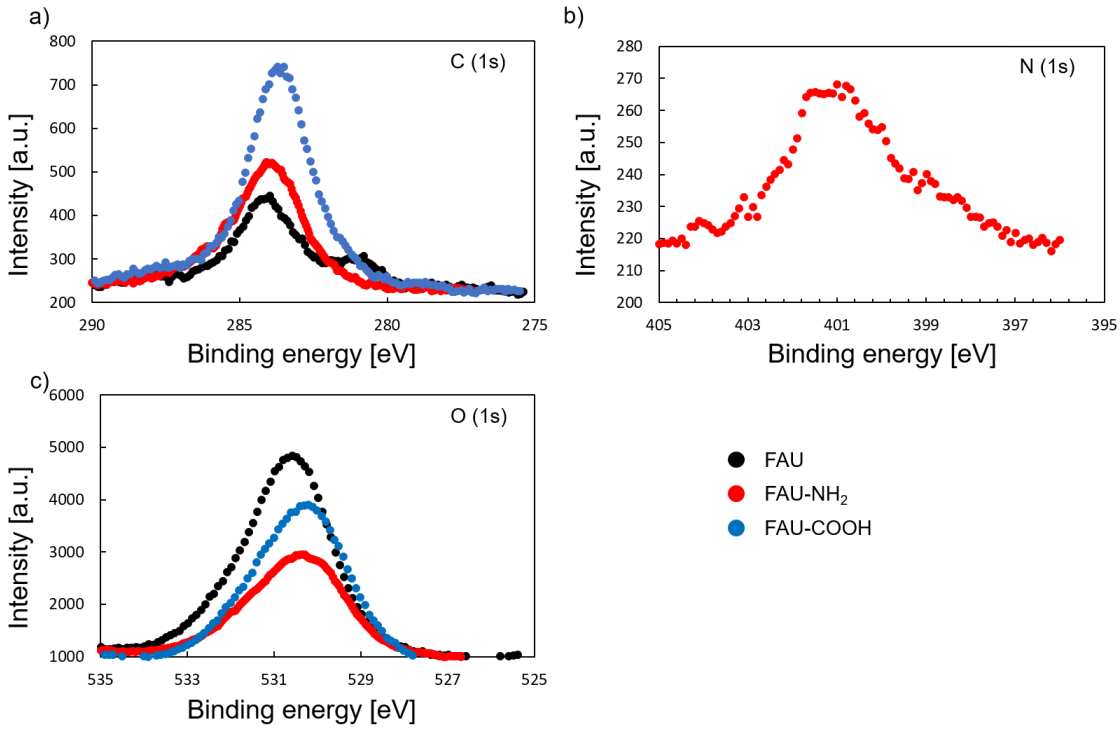

Figure 6. XPS spectra of both FAU, FAU-NH_2, and FAU-COOH depicting the carbon 1s (a), nitrogen 1s (b), and oxygen 1s (c) respectively.

3.2. Efficiency of composites

The thermomechanical properties of composites are tightly related to the interactions between particles, and the polymer/protein chains[7]. Therefore, functionalized and neat zeolites were mixed with gelatin solutions at different percentages (i.e. 5 and 15 %) to investigate any improvement of the thermal properties of the gels. After a given period in an oven heated up at 37 °C, tubes containing the composites were turned upside down, flowing samples were considered as unstable (**Figure 7**). One can observe that none of the tested conditions were stable more than 30 minutes at 37 °C. The most stable samples corresponding to either FAU-COOH and FAU-NH2 at 15 %, combined with gelatin at 15 %. Neat FAU was stable only for 20 min. Hence, surface functionalization of zeolites was inefficient to form stable composite under physiological conditions. It was previously found that thermomechanical properties of composites strongly depend on the aspect ratio of the particles, their dispersion state, and their strength of interaction with the polymer[56]).

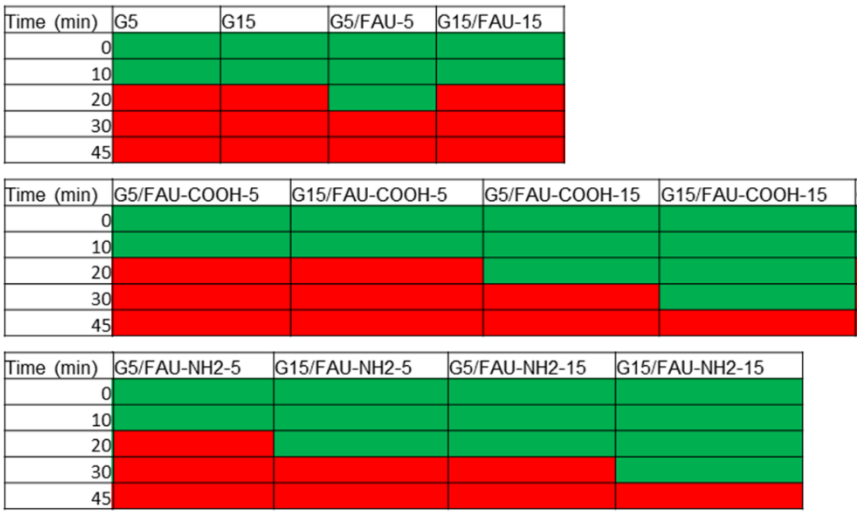

Figure 7. Summay of stability tests of composites at 37 °C determine by the upside-down method of the tubes. Green grids refer to stable conditions, and red grids to unstable ones. Samples were named using the following nomenclature GX/FAU-YYYY-Z, where X corresponds to the gelatin concentration (wt.%), Y letters indicate the type of surface groups (COOH or NH_2), and Z stands for the zeolite concentration (wt.%). All samples were prepared in PBS as the solvent.

If aspect ratio of zeolites can be controlled from the synthesis route[57] this effect is hindered by the large crystal aggregates (**Figure 1a**). Moreover, electrostatic interactions resulting from surface functionalization were not found to be strong enough to reinforce gelatin/zeolite composites. To our best knowledge, no stable composite based on zeolite and gelatin at 37 °C has been reported yet, or only by the aid of additional crosslinking[58,30].
The coupling of *N,N*-(3-dimethylaminopropyl)-*N'*-ethyl-carbodiimide hydrochloride (EDC) with sulfo-*N*-hydroxysuccinimide (NHS) is a broadly used method to crosslink proteins intended to biological applications[59]. The classical reaction path involves the activation of carboxylic groups by carbodiimide, which can further react with primary amines located on the gelatin chains. Hence, FAU-COOH are appealing for direct bridging with gelatin. On the other hand, FAU crystals alone are not expected to be sensitive to this coupling, but will rather be encapsulated within the gelatin matrix after crosslinking. As gelatin harbors both free carboxylic acid groups (aspartic and glutamic acids), and primary amines (lysine, and hydroxylysine)[60], gelatin alone could be crosslinked via EDC/NHS. Hence one can expect a direct binding of FAU-COOH with gelatin upon EDC/NHS treatment, along with some gelatin-gelatin linkages, and FAU to be only embedded into crosslinked gelatin. Lastly, FAU-NH_2 could be linked to gelatin after activation of carboxylic acids residues on gelatin, whose amount is relatively large in comparison with the other amino acids of type A gelatin[61].
FTIR spectra of composites with gelatin alone, or with FAU, NH2-FAU, and COOH-FAU are shown in **Figure 8**. The amine bond resulting from EDC/NHS treatment appeared at 1170 cm^{-1} in all the crosslinked samples[62], confirming that the reaction occurred. The footprint of zeolite crystals can be seen in the 980 cm^{-1} region attributed to the Si-O-Si vibration, which is absent on samples containing gelatin solely.

The effect of EDC/NHS treatment was evaluated by thermal treatment at 37 °C in an oven (**Figure 9a**), spanning several gelatin (5 and 15 %) and zeolite (5 and 15 %) concentrations in a combinatorial manner. All samples were stable for 24 h as a result of the chemical crosslinking. The thermal behavior was investigated further through DSC analysis (**Figure 9b-d**). Gelatin hydrogels alone, or loaded with zeolites without EDC/NHS displayed an endothermal peak at 38,25 °C for pristine gelatin, 37,76 °C for FAU-COOH, 38,89 °C for FAU-NH2, and 38,87 °C for FAU suggesting negligible changes in the gel-sol transition of the composites, even in presence of zeolites, without additional crosslinks. Any displacement of the endothermic peak, or of its integrated area, is interpreted as the evolution of the stability of the triple helix, which depends on gelatin concentration, or on the length of the helixes[63]. As gelatin concentration remained constant, and crystal sizes (**Figure 1c**) are too large to be intercalated in the helixes, no particular evolution was expected at a first glance. Another cause widely related to shifting of this peak can results from the interaction between the dispersed particles, and the gelatin chains, which was not observed neither. This agrees with the stability tests in **Figure 7**, and follows the same trend as previous work by Fernandes *et al.*[64] for gelatin-sepiolite composites. In another study[65], gelatin composite was prepared with magnetite nanoparticles, leading to a 6 °C increase of melting temperature of gelatin, attributed to an increase in crosslink density by the nanoparticles. The thermal stability of composites is therefore related to various parameters including surface chemistry of the fillers, the aspect ratio[55], or the relative amount of particles with respect to polymer. In the present work, thermal properties were recorded for composites with 15 % gelatin, and 15 % zeolites while previous tests at lower particle concentrations did not induce significant change of the DSC thermogram (data not shown). After treatment with EDC/NHS, the characteristic peak related to gel-sol transition vanished for all samples. Since the transition is related to the reversible helix-to-coil transition of gelatin stabilized by physical bonds, the chemical crosslinking has immobilized the triple helix, and therefore, increased the thermal stability of this composite.

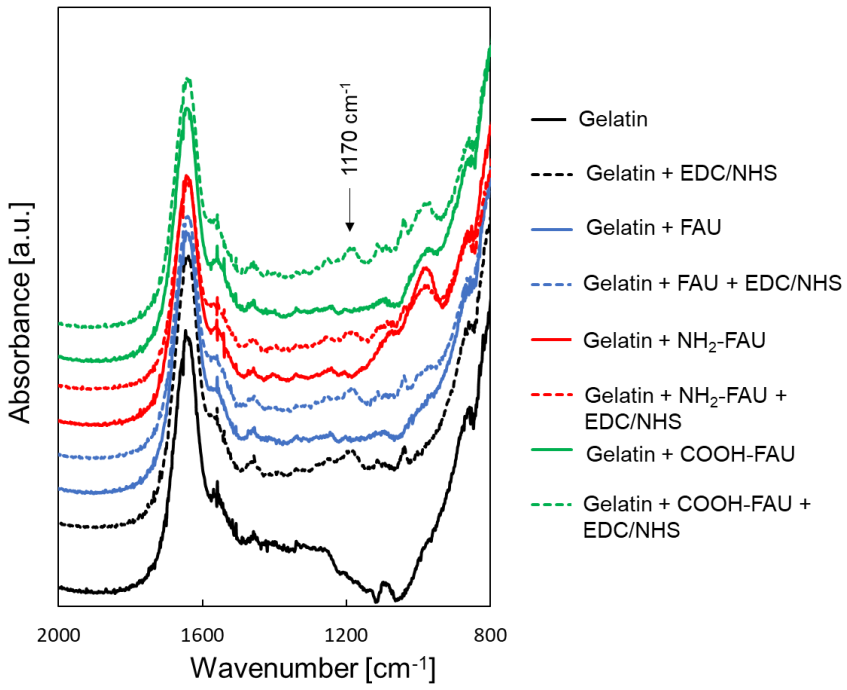

Figure 8. FTIR-ATR spectra showing the effect of EDC/NHS treatment on composites prepared with gelatin only, or by mixing gelatin with either FAU, NH_2-FAU, or COOH-FAU.

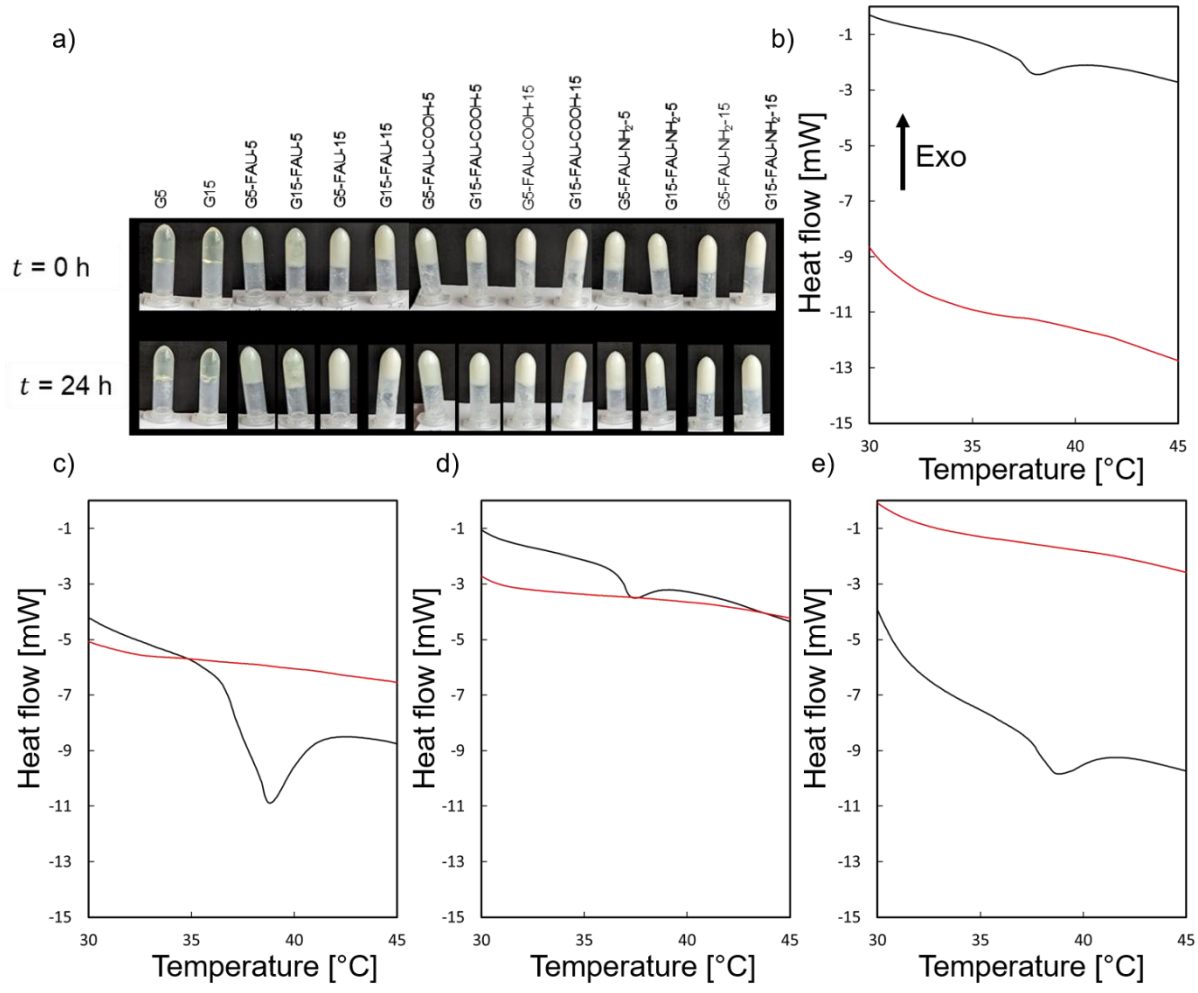

Figure 9. Stability tests at 37 °C performed via the upside-down method, directly after having obtained the composites (t = 0h), and after 24 h. All conditions were crosslinked using EDC/NHS. Samples were named using the following nomenclature GX/FAU-YYYY-Z, where X corresponds to the gelatin concentration (wt.%), Y letters indicate the type of surface groups (COOH or NH_2), and Z stands for the zeolite concentration (wt.%). All samples were prepared in PBS as the solvent. DSC curves obtained with gelatin concentration of 15 wt.%, and for 15 wt.% of the given zeolites. b) is refers to neat gelatin, c) gelatin + FAU, d) gelatin + FAU-COOH, and

e), gelatin + FAU-NH_2. Black curve represents the conditions without EDC/NHS, and red curves the same condition, with EDC/NHS treatment.

3.3. Biological properties of composites

The resulting composites were intended to form supports for soft tissue engineering applications, such as chronic wounds. Only the composite treated by EDC/NHS were chosen, and viability of macrophage-derived THP-1 cells was evaluated as a relevant cell source to estimate the biocompatibility of the composites. Since macrophages are among the first cell source arriving at the tissue/implant interface, their function reflects the inflammatory state induced by the composites, and determine the long-term outcomes[66]. Considering the surface functionalization, and crosslinking steps involved in the formulation of the composites, leakage of cytotoxic compounds should be detected. No toxicity associated to gelatin was expected in line with our previous study[5]. As depicted on **Figure 10**, cell viability was followed for 6 days, and all the zeolite-loaded composites (FAU, FAU-NH_2, and FAU-COOH) were biocompatible, showing no reduced viability with respect to control over the whole period, displaying between 70-80 % viability for all conditions. Early work by Dahm *et al.*[17] already showed that Y-zeolites (i.e. faujasite) did not induce cytotoxic effect on THP-1 cells. The presence of aluminum in the framework could increase the mitochondrial activity of THP-1 cells due to enzymatic processes, to Aluminum released from dealuminated zeolites was shown to increase the mitochondrial activity of THP-1 cells[67] with time due to enzymatic processes. As shown in **Figure 10**, the mitochondrial activity of THP-1 cells remained fairly constant over the 6 days of the experiment, which corroborates that no harmful compounds were released. Moreover, the surface of zeolites is known to promote protein adsorption including albumin, fibrinogen, or apolipoprotein[68], which subsequently mediate cell adhesion, and may contribute to improve to biocompatibility of zeolites. In this work, as zeolites are embedded into gelatin, direct cell-zeolite contacts may be limited, and adsorbed proteins may even mitigate any harmful effect. In addition, Surmaitis *et al.*[69] demonstrated that mitochondrial activity of cells is increased on poorly adhesive substrates up to three days after seeding, due to excessive secretion of extracellular matrix. This further support the fact that the composites hereof do not impair cell functions.

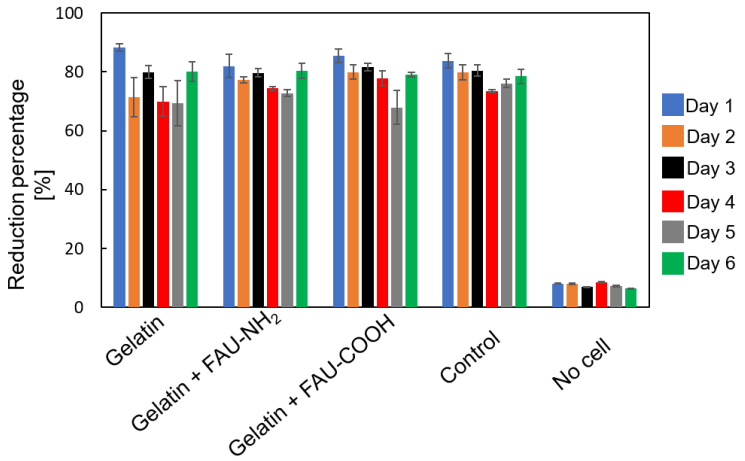

Figure 10. Evaluation of THP-1 cell viability at different time points using Alamar blue® kit. Control condition is related to cell cultured in classical RPMI medium. Results are expressed as mean ± SD, n= 3.

Conclusion

FAU zeolite nanocrystals were successfully synthesized, and formed submicrometric colloids which were stable in PBS. In order to yield stable gelatin/zeolite composites, the surface of the resulting crystals was subsequently modified using APTES to graft amine groups, and TESPA to graft carboxylic groups. The latter functionalization approach was not reported yet. Both surfaces treatments were then used for covalently bind gelatin chains to zeolites using EDC/NHS coupling, yielding to stable composites. Lastly, the biocompatibility of the gels was tested by seeding macrophage-derived THP-1 cells, showing no adverse effect. An ongoing study is dedicated to probe the mechanical properties of these composites, and to deeper investigation of the inflammatory profile of THP-1 cells.

AUTHOR INFORMATION

Corresponding Author

* Dr. Gaëtan Lutzweiler, gaetanlutweiler@gmail.com
* Dr. Benoît Louis, blouis@unistra.fr

Author Contributions

The manuscript was written through contributions of all authors who contributed equally to this work. All authors have given approval to the final version of the manuscript.

Funding Sources

The FTIR spectrometer was financed by the Région Normandie (FEDER RIN Green Chem). This project was partially funded by the Fondation de l'Avenir, Paris, France (N° AP-RM-22-027).

ABBREVIATIONS

FAU, faujasite, PP polypropylene, APTES, 3-(aminopropyl)triethoxysilane, TESPA, 5-(triethoxysilyl)pentanoic acid.

REFERENCES

1. Botelho, E. C.; Rezende, M. C.; Lauke, B. Mechanical behavior of carbon fiber reinforced polyamide composites. *Compos. Sci. Technol.* 2003, 63(13), 1843-1855.
2. Hassan, T.; Salam, A.; Khan, A.; Khan, S. U.; Khanzada, H.; Wasim, M.; Khan, M. Q.; Kim, I. S. Functional nanocomposites and their potential applications: A review. *J. Polym. Res*. 2021, *28*, 1-22.
3. Karki, S.; Gohain, M. B.; Yadav, D.; Ingole, P. G. Nanocomposite and bio-nanocomposite polymeric materials/membranes development in energy and medical sector: A review. *Int. J. Biol. Macromol*. 2021, *193*, 2121-2139.
4. Ji, B.; Gao, H. Mechanical principles of biological nanocomposites. *Annu. Rev. Mater. Res.* 2010, *40*, 77-100.
5. Barthès, J.; Lagarrigue, P.; Riabov, V.; Lutzweiler, G.; Kirsch, J.; Muller, C.; Courtial, E. J.; Marquette, C.; Projetti, F.; Kzhyskowska, J.; Lavalle, P.; Vrana, N. E.; Dupret-Bories, A. Biofunctionalization of 3D-printed silicone implants with immunomodulatory hydrogels for controlling the innate immune response: An in vivo model of tracheal defect

repair. *Biomaterials*. 2021, *268*, 120549.
6. Miyazaki, S.; Karino, T.; Endo, H.; Haraguchi, K.; Shibayama, M. Clay concentration dependence of microstructure in deformed poly (N-isopropylacrylamide)− clay nanocomposite gels. *Macromolecules*. 2006, *39*(23), 8112-8120.
7. Dannert, C.; Stokke, B. T.; Dias, R. S. Nanoparticle-hydrogel composites: from molecular interactions to macroscopic behavior. *Polymers*. 2019, *11*(2), 275.
8. Bardajee, G. R.; Hooshyar, Z.; Asli, M. J.; Shahidi, F. E.; Dianatnejad, N. Synthesis of a novel supermagnetic iron oxide nanocomposite hydrogel based on graft copolymerization of poly ((2-dimethylamino) ethyl methacrylate) onto salep for controlled release of drug. *Mater. Sci. Eng. C*. 2014, *36*, 277-286.
9. Darvas, F.; Mezey, P. G.; Dormán, G.; Buchholcz, B.; Janáky, C.; Jones, R. V.; Mezohegyi, G. Chemistry-Related Innovations in Space, Benefits of Flow Chemistry. *In-Space Manufacturing and Resources: Earth and Planetary Exploration Applications*. 2022, (eds V. Hessel, J. Stoudemire, H. Miyamoto and I.D. Fisk), p. 109-140.
10. Gomes, E. S.; Lutzweiler, G.; Losch, P.; Silva, A. V.; Bernardon, C.; Parkhomenko, K.; Pereira, M. M.; Louis, B. Strategy to design zeolite catalysts in the presence of biomass. *Microporous Mesoporous Mater*. 2017, *254*, 28-36.
11. Mintova, S.; Jaber, M.; Valtchev, V. Nanosized microporous crystals: emerging applications. *Chem. Soc. Rev*. 2015, *44*(20), 7207-7233.
12. Awala, H.; Gilson, J. P.; Retoux, R.; Boullay, P.; Goupil, J. M; Valtchev, V.; Mintova, S. Template-free nanosized faujasite-type zeolites. *Nat. Mater*. 2015, *14*(4), 447-451.
13. Anfray, C.; Komaty, S.; Corroyer-Dulmont, A.; Zaarour, M.; Helaine, C.; Ozcelik, H.; Allioux, C.; Toutain, J.; Goldyn, K.; Petit, E.; Bordji, K.; Bernaudin, M.; Valtchev, V.; Touzani, O.; Mintova, S.; Valable, S. *Biomaterials*. 2020, 257, 120249.
14. Lutzweiler, G.; Zhang, Y.; Gens, F.; Echalard, A.; Ladam, G.; Hochart, J.; Janicot, T.; Mofaddel, N.; Louis, B. Deciphering the role of faujasite-type zeolites as a cation delivery platform to sustain the functions of MC3T3-E1 pre-osteoblastic cells. *Mater. Adv.* 2022, *3*(23), 8616-8628.
15. Tosheva, L.; Brockbank, A.; Mihailova, B.; Sutula, J.; Ludwig, J.; Potgieter, H.; Verran, J. Micron-and nanosized FAU-type zeolites from fly ash for antibacterial applications. *J. Mater. Chem.* 2012, *22*(33), 16897-16905.
16. Vilaça, N.; Bertão, A. R.; Prasetyanto, E. A.; Granja, S.; Costa, M.; Fernandes, R.; Figueiredo, F.; Fonseca, A. M.; De Cola, L.; Baltazar, F.; Neves, I. C. Surface functionalization of zeolite-based drug delivery systems enhances their antitumoral activity in vivo. *Mater. Sci. Eng. C. 2021*, *120*, 111721.
17. Dahm, Å.; Eriksson, H. Ultra-stable zeolites—a tool for in-cell chemistry. 2004, *J. Biotechnol*, *111*(3), 279-290.
18. Mittal, H.; Babu, R.; Dabbawala, A. A.; Stephen, S.; Alhassan, S. M. Zeolite-Y incorporated karaya gum hydrogel composites for highly effective removal of cationic dyes. *Colloids Surf. A: Physicochem. Eng*. 2020, *586*, 124161.
19. S Dragan, E.; V Dinu, M. Progress in polysaccharide/zeolites and polysaccharide hydrogel composite sorbents and their applications in removal of heavy metal ions and dyes. *Curr. Green Chem.* 2015, *2*(4), 342-353.
20. Larlus, O.; Mintova, S.; Bein, T. Environmental syntheses of nanosized zeolites with high yield and monomodal particle size distribution. *Microporous Mesoporous Mater. 2006*, *96*(1-3), 405-412.
21. Mendoza-Castro, M. J.; Qie, Z.; Fan, X.; Linares, N.; García-Martínez, J. Tunable hybrid zeolites prepared by partial interconversion. *Nat. Commun*. 2023, *14*(1), 1256.

22. Oleksiak, M. D.; Soltis, J. A.; Conato, M. T.; Penn, R. L.; Rimer, J. D. (2016). Nucleation of FAU and LTA zeolites from heterogeneous aluminosilicate precursors. *Chem. Mater. 2016, 28*(14), 4906-4916.
23. Israelachvili, J. N. (2011). *Intermolecular and surface forces*. Academic press.
24. Cruz, R. C.; Segadães, A. M.; Oberacker, R.; Hoffmann, M. J. Double layer electrical conductivity as a stability criterion for concentrated colloidal suspensions. *Colloids Surf. A Physicochem*. 2017, *520*, 9-16.
25. Gözcü, O.; Kayacı, H. U.; Dou, Y.; Zhang, W.; Hedin, N.; Jasso-Salcedo, A. B.; Kaiser, A.; Çinar Aygün, S. Colloidal Stabilization of Submicron-Sized Zeolite NaA in Ethanol–Water Mixtures for Nanostructuring into Thin Films and Nanofibers. *Langmuir*. 2022, *39*(1), 192-203.
26. Kirschhock, C. E.; Kremer, S. P.; Vermant, J.; Van Tendeloo, G.; Jacobs, P. A.; Martens, J. A. Design and synthesis of hierarchical materials from ordered zeolitic building units. *Chem. Eur. J. 2005*, *11*(15), 4306-4313.
27. Persson, A. E.; Schoeman, B. J.; Sterte, J.; Otterstedt, J. E. The synthesis of discrete colloidal particles of TPA-silicalite-1. *Zeolites*. 1994, *14*(7), 557-567.
28. Zhang, Y.; Liu, S.; Chen, H.; Josien, L.; Schrodj, G.; Simon-Masseron, A.; Lalevée, J. Development of a Zeolite/Polymer-Based Hydrogel Composite through Photopolymerization for 3D Printing Application. *Macromol Mater Eng. 2021*, *306*(8), 2100129.
29. Fathi, P.; Sikorski, M.; Christodoulides, K.; Langan, K.; Choi, Y. S.; Titcomb, M., Ghodasara, A., Omasiri. W.; Hemi, T.; Mert, V.; Behrens, A.; Kofinas, P. Zeolite-loaded alginate-chitosan hydrogel beads as a topical hemostat. *J. Biomed. Mater. Res. Part B*. 2018, *106*(5), 1662-1671.
30. Ninan, N.; Grohens, Y.; Elain, A.; Kalarikkal, N.; Thomas, S. Synthesis and characterisation of gelatin/zeolite porous scaffold. *Eur. Polym. J. 2013, 49*(9), 2433-2445.
31. Larsen, S. C. Nanocrystalline zeolites and zeolite structures: synthesis, characterization, and applications. *J. Phys. Chem. C*. 2007, *111*(50), 18464-18474.
32. Younesi, H.; Asghari, S.; Pasha, G. F.; Tajbakhsh, M. Ugi-modified nano NaY zeolite for the synthesis of new 1, 5-dihydro-2H-pyrrol-2-ones under mild conditions. *Appl. Organomet. Chem. 2023*, e7127.
33. Kehr, N. S.; Riehemann, K.; El-Gindi, J.; Schäfer, A.; Fuchs, H.; Galla, H. J.; & De Cola, L. Cell Adhesion and Cellular Patterning on a Self-Assembled Monolayer of Zeolite L Crystals. *Adv. Funct. Mater. 2010*, *20*(14), 2248-2254.
34. Feinle, A.; Leichtfried, F.; Straßer, S.; Hüsing, N. Carboxylic acid-functionalized porous silica particles by a co-condensation approach. *J. Sol-Gel Sci. Technol. 2017*, *81*, 138-146.
35. Mokgehle, T. M.; Gitari, W. M.; Tavengwa, N. T. Synthesis of di-carboxylic acid functionalized zeolites from coal fly ash for Cd (II) removal from acid mine drainage using column studies approach. *J. Environ. Chem. Eng. 2019*, *7*(6), 103473.
36. Arkles, B. (1977). Tailoring surfaces with silanes. *Chemtech*, *7*, 766-778.
37. Johansson, U.; Holmgren, A.; Forsling, W.; Frost, R.L. Adsorption of silane coupling agents onto kaolinite surfaces. *Clay Miner.* 1999, 34, 239-246.
38. Lee, L.H.; J. Wettability and conformation of reactive polysiloxanes. *Coll. Surf. Sci.* 1968, 27, 751-760.
39. Sindorf, D.W.; Maciel, G.E. 29Si NMR Study of dehydrated/rehydrated Silica Gel using CP and MAS. *J. Am. Chem. Soc.* 1983, 105, 1487-1493.
40. Philipse, A.P.; Vrij, A. Preparation and properties of nonaqueous model dispersions of chemically modified, charged silica spheres. *J. Coll. Interf. Sci.* 1989, 128, 121-136.
41. Derouet, D.; Forgeard, S.; Brosse, J.C.; Emery, J.; Buzare, J. Y. Application of Solid-State NMR (13C and 29Si CP/MAS NMR) Spectroscopy to the Characterization of Alkenyltrialkoxysilane and Trialkoxysilyl-Terminated Polyisoprene Grafting onto Silica

Microparticles. *J. Polym. Sci. A.* 1998, 36, 437-453.
42. Kim, S. G.; Hyeon, D. H. Chun, J. H.; Chun, B. H.; Kim, S. H. Nanocomposite poly (arylene ether sulfone) reverse osmosis membrane containing functional zeolite nanoparticles for seawater desalination. *J. Membr. Sci. 2013*, *443*, 10-18.
43. Nik, O. G.; Nohair, B.; Kaliaguine, S. Aminosilanes grafting on FAU/EMT zeolite: Effect on CO2 adsorptive properties. *Microporous Mesoporous Mater. 2011*, *143*(1), 221-229.
44. Qin, Z.; Cychosz, K. A.; Melinte, G.; El Siblani, H.; Gilson, J. P.; Thommes, M.; Fernandez, C.; Mintova, S.; Valtchev, V. Opening the cages of faujasite-type zeolite. *J. Am. Chem. Soc. 2017*, *139*(48), 17273-17276.
44. Sypabekova, M.; Hagemann, A.; Rho, D.; Kim, S. 3-Aminopropyltriethoxysilane (APTES) Deposition Methods on Oxide Surfaces in Solution and Vapor Phases for Biosensing Applications. *Biosens. 2022*, *13*(1), 36.
45. Laurenti, J. B.; Zazeri, G.; Povinelli, A. P. R.; de Godoy, M. F.; Braile, D. M.; da Rocha, T. R. F.; D'Amico, E. A.; Nery, J. G. Enhanced pro-coagulant hemostatic agents based on nanometric zeolites. *Microporous Mesoporous Mater. 2017*, *239*, 263-271.
46. Joseph, E.; Singhvi, G. Multifunctional nanocrystals for cancer therapy: a potential nanocarrier. *Nanomaterials for drug delivery and therapy*. 2019, 91-116.
47. Mahmoodi, N. M.; Saffar-Dastgerdi, M. H. Zeolite nanoparticle as a superior adsorbent with high capacity: Synthesis, surface modification and pollutant adsorption ability from wastewater. *Microchem. J. 2019, 145*, 74-83.
48. Jabbari-Gargari, A.; Moghaddas, J.; Hamishehkar, H.; Jafarizadeh-Malmiri, H. Carboxylic acid decorated silica aerogel nanostructure as drug delivery carrier. *Microporous Mesoporous Mater*. 2021, *323*, 111220.
49. Lu, Y.; Huang, X.; Wang, S.; Li, B.; Liu, B. Nanoconfinement-Enhanced Electrochemiluminescence for in Situ Imaging of Single Biomolecules. *ACS nano*. 2023, *17*(4), 3809-3817.
50. Li, Z.; Luppi, G.; Geiger, A.; Josel, H. P.; De Cola, L. Bioconjugated fluorescent zeolite L nanocrystals as labels in protein microarrays. *Small*. 2011, *7*(22), 3193-3201.
51. Rao, X.; Tatoulian, M.; Guyon, C.; Ognier, S.; Chu, C.; Abou Hassan, A. A comparison study of functional groups (amine vs. Thiol) for immobilizing aunps on zeolite surface. *Nanomater. 2019, 9*(7), 1034.
52. Cueto-Díaz, E. J.; Castro-Muñiz, A.; Suárez-García, F.; Gálvez-Martínez, S.; Torquemada-Vico, M. C.; Valles-González, M. P.; Mateo-Martí, E. Aptes-based silica nanoparticles as a potential modifier for the selective sequestration of CO2 gas molecules. *Nanomater. 2021, 11*(11), 2893.
53. Ramos-Martinez, V. H.; Ramirez-Vargas, E.; Medellin-Rodriguez, F. J.; Ávila-Orta, C. A.; Gallardo-Vega, C. A.; Jasso-Salcedo, A. B.; Andrade-Guel, M. L. Zeolite 13X modification with gamma-aminobutyric acid (GABA). *Microporous Mesoporous Mater. 2020*, *295*, 109941.
54. Kawai, T., Tsutsumi, K. A study on the surface silanol groups developed by hydrothermal and acid treatment of faujasite type zeolites. *J Colloid Interface Sci*. 1999, *212*(2), 310-316.
55. Panchenko, V. N., Borbáth, I., Timofeeva, M. N., & Gőbölös, S. Amine-modified silica NH2–(CH2) x–SiO2 (x= 0, 2, 3) as support for cobalt-substituted polyoxometalate TBA4HPW11CoO39: Effect of the nature of the support on the oxidation activity. *J Mol Catal A Chem*. 2010, *319*(1-2), 119-125.
56. Rao, Y. Gelatin–clay nanocomposites of improved properties. *Polymer*. 2007, *48*(18), 5369-5375.
57. Louis, B.; Gomes, E.S.; Losch, P.; Lutzweiler, G.; Coelho, T.; Faro Jr, A.; Pinto, J.F.; Cardoso, C.S.; Silva, A.V.; Pereira, M.M. Biomass-assisted zeolite syntheses as a tool for designing new

acid catalysts. *ChemCatChem.* 2017, 9, 2065–2079.
58. Marín, T.; Montoya, P.; Arnache, O.; Pinal, R.; Calderón, J. Development of magnetite nanoparticles/gelatin composite films for triggering drug release by an external magnetic field. *Mater. Des. 2018, 152*, 78-87.
59. Goodarzi, H.; Jadidi, K.; Pourmotabed, S.; Sharifi, E.; Aghamollaei, H. Preparation and in vitro characterization of cross-linked collagen–gelatin hydrogel using EDC/NHS for corneal tissue engineering applications. *Int. J. Biol. Macromol. 2019*, *126*, 620-632.
60. Kuijpers, A. J.; Engbers, G. H.; Krijgsveld, J.; Zaat, S. A.; Dankert, J.; Feijen, J. Cross-linking and characterisation of gelatin matrices for biomedical applications. *J. Biomater. Sci. Polym. Ed. 2000*, *11*(3), 225-243.
61. Hafidz, R. M. R. N.; Yaakob, C. M.; Amin, I.; Noorfaizan, A. Chemical and functional properties of bovine and porcine skin gelatin. *Int. Food Res. J. 2011*, *18*(2), 787-791.
62. Gornall, J. L.; Terentjev, E. M. Helix–coil transition of gelatin: helical morphology and stability. *Soft Matter*. 2008, *4*(3), 544-549.
63. Fernandes, F. M.; Manjubala, I.; Ruiz-Hitzky, E. Gelatin renaturation and the interfacial role of fillers in bionanocomposites. *Phys. Chem. Chem. Phys. 2011*, *13*(11), 4901-4910.
64. Yang, I. H., Kuan, C. Y., Chen, Z. Y., Li, C. H., Chi, C. Y., Lin, Y. Y., Liang, Y. J., Kuo, W. T., Li, Y. A., Lin, F. H. Engineered cell-laden thermosensitive poly (N-isopropylacrylamide)-immobilized gelatin microspheres as 3D cell carriers for regenerative medicine. *Mater. Today Bio.* 2022, *15*, 100266.
65. Marín, T.; Montoya, P.; Arnache, O.; Pinal, R.; Calderón, J. Development of magnetite nanoparticles/gelatin composite films for triggering drug release by an external magnetic field. *Mater. Des. 2018*, *152*, 78-87.
66. McCanna, D. J.; Barthod-Malat, A. V.; Gorbet, M. B. In vitro methods of assessing ocular biocompatibility using THP-1-derived macrophages. *Cutan. Ocul. Toxicol*. 2015, *34*(2), 89-100.
67. Ohlsson, L., Exley, C., Darabi, A., Sandén, E., Siesjö, P., & Eriksson, H. Aluminium based adjuvants and their effects on mitochondria and lysosomes of phagocytosing cells. *J. Inorg. Biochem.* 2013, *128*, 229-236.
68. Rahimi, M.; Ng, E. P.; Bakhtiari, K.; Vinciguerra, M.; Ahmad, H. A.; Awala, H.; Mintova, S.; Daghighi, M.; Rostami, F. B.; de Vries, M.; Matazacker, M. M.; Peppelenbosch, M. P.; Mahmoudi, M.; Rezaee, F. *Sci. Rep*. 2015, *5*(1), 1-12.
69. Surmaitis, R. L.; Arias, C. J; Schlenoff, J. B. Stressful surfaces: Cell metabolism on a poorly adhesive substrate. *Langmuir*. 2018, *34*(9), 3119-3125.

Table of content (TOC)

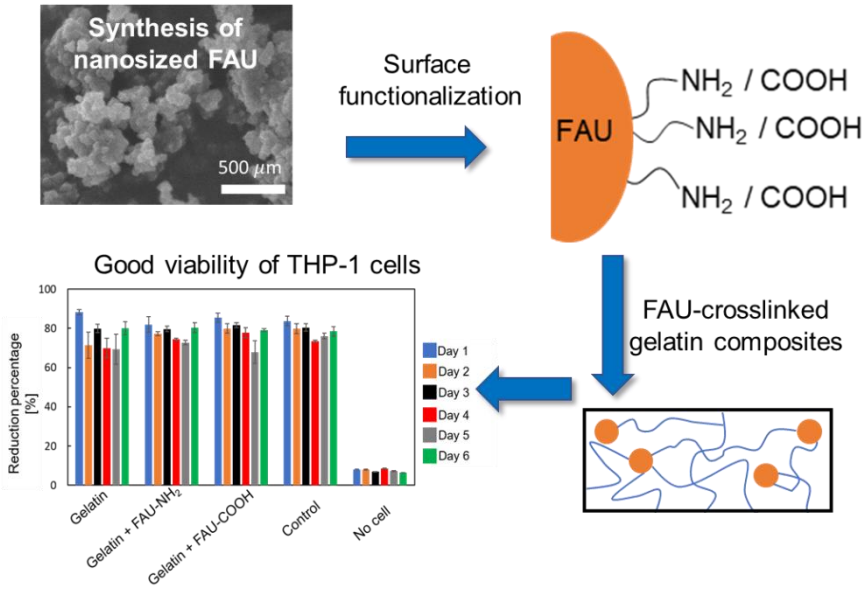
Synthesis of nanosized FAU
500 μm
Surface functionalization
FAU
NH2 / COOH
NH2 / COOH
NH2 / COOH
FAU-crosslinked gelatin composites
Good viability of THP-1 cells
Reduction percentage [%]
100
80
60
40
20
0
Day 1
Day 2
Day 3
Day 4
Day 5
Day 6
Gelatin
Gelatin + FAU-NH2
Gelatin + FAU-COOH
Control
No cell